THE JOURNAL OF PHYSICAL CHEMISTRY A

Article

pubs.acs.org/JPCA

Gas-Phase Reaction between CF_2O and $CF_3C(O)OH$: Characterization of $CF_3C(O)OC(O)F$

Matias Berasategui, Gustavo A. Argüello, and Maxi A. Burgos Paci*

Instituto de Investigaciones en Físico Química de Córdoba (INFIQC) CONICET-UNC, Departamento de Físico Química, Facultad de Ciencias Químicas, Universidad Nacional de Córdoba, Ciudad Universitaria, X5000HUA Córdoba, Argentina

Supporting Information

ABSTRACT: The thermal decomposition of trifluoroacetic acid and carbonyl fluoride (CF_2O) has been extensively studied because of their importance in the oxidation of hydrochlorofluorocarbons in the atmosphere. We hitherto present the study of the thermal reaction between these two molecules. The reaction mechanism was studied using Fourier transform infrared spectroscopy in the temperature range of 513−573 K. The reaction proceeds homogeneously in the gas phase through the formation of a reaction intermediate, here characterized as $CF_3C(O)OC(O)F$ (detected for the first time in this work), the major final products being $CF_3C(O)F$, HF, and CO_2. We demonstrate that the reaction is first-order respect to each reagent, second-order global and the mechanism consists of two steps, the first being the rate-determining one. The E_a = 110.1 ± 6.1 kJ mol^{-1} and A = (1.2 ± 0.2) × 10^{-12} cm^3 molec^{-1} s^{-1} values were obtained from the experimental data. The low activation energy is explained by the hydrogen-bond interactions between the −OH group of the acid and the F atom of the CF_2O. First-principles calculations at the G4MP2 level of theory were carried out to understand the dynamics of the decomposition. Thermodynamic activation values found for this reaction are as follows: $\Delta H^{\ddagger}$ = 105.6 ± 6.4 kJ mol^{-1}, $\Delta S^{\ddagger}$ = −88.6 ± 9.7 J mol^{-1} K^{-1}, and $\Delta G^{\ddagger}$ = 153.7 ± 13.5 kJ mol^{-1}. The comparison between theory and experimental results showed excellent similarities, thus strengthening the proposed mechanism.

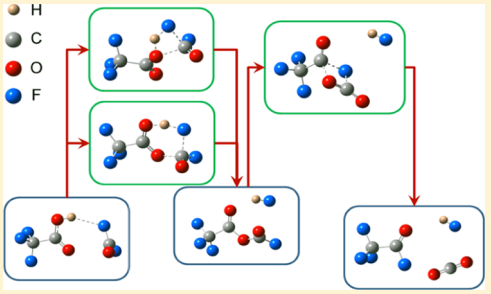

1. INTRODUCTION

Carbonyl fluoride (CF_2O) and trifluoroacetic acid (TFA) could account for almost a third of the inorganic fluorinated compounds in the atmosphere,[1−4] and it is expected that their concentrations will increase in the future.[5−7] This is due to the current widespread use of replacements, that is, hydrofluorocarbons and hydrofluoroethers, as well as the past use of chlorofluorocarbons.[8−13] Though their concentrations are still far from becoming an environmental problem (its mutual reaction has not yet become an environmental issue), the reaction is of interest from the point of view of fluorine as well as physical chemistry. It affords a new fluorooxygenated compound to be synthesized and characterized and allows fundamental kinetic parameters to be known. It is widely accepted that perfluorinated carbonyl compounds have proved to be valuable tools in the study of radical reactions of atmospheric species.[14−17]

Gangloff et al.[18] studied the thermal decomposition of CF_2O. The only probable reaction path is the C−F bond scission. The activation energy for this reaction is 323 ± 13 kJ mol^{-1}. Modica et al.[19] proposed that CF_2O may react with CO to produce covalent organic framework radicals, but this reaction is completely displaced toward reagents. Ashworth et al. studied the thermal decomposition of $CF_3C(O)OH$ in the gas phase by Fourier transform infrared (FTIR) spectroscopy, with a stainless steel IR gas cell equipped with silver chloride windows. The main products found for this reaction were CF_3H and CO_2.[20]

The reactions of Cl/F and OH with $CF_3C(O)OH$ were studied by Wallington and Hurley,[21] concluding that these reactions constitute a minor atmospheric fate of $CF_3C(O)OH$ and that the major atmospheric removal mechanism would be wet and dry deposition, which probably occurs on a time scale of the order of several weeks.[5,22,23] However, little is known about the reaction of the acid with other stable molecules that have longer lifetimes than the radicals mentioned.

Our group has extensive experience in the synthesis of fluorocarbooxygenated molecules.[24−27] In particular, studies have been carried out on thermal reactions in the gas phase that afforded new species that have been characterized by different techniques and rigorously verified by the kinetic mechanisms proposed.[28−30]

We hereafter present a thorough study of the thermal reaction between $CF_3C(O)OH$ and CF_2O at different temperatures and pressures, which was also supported by high-level ab initio calculations. The results from the kinetic study are discussed with respect to the characterization of $CF_3C(O)OC(O)F$ by FTIR spectroscopy.

Received: January 29, 2019
Revised: April 29, 2019
Published: May 3, 2019

DOI: 10.1021/acs.jpca.9b00899
J. Phys. Chem. A XXXX, XXX, XXX−XXX

2. EXPERIMENTAL SECTION

2.1. Instrumentation. *2.1.1. Vibrational Spectroscopy.* Gas-phase IR spectra in the range of 4500−400 cm^{-1} were recorded with a resolution of 2 cm^{-1} from 32 coadded interferograms using a FTIR instrument (Bruker IFS66V) equipped with a photoconductive MCT detector and OPUS software.

2.1.2. IR Cells. In order to achieve the desired temperatures required to initiate the reactions (513−573 K), we used an electrically heated stainless steel cell (optical path length 100 mm) with silicon windows, connected to a temperature controller (Instrelec NC201-V) regulated from a thermocouple. The whole system (cell, resistors, and thermocouple) was coated with a ceramic fiber to isolate it from the environment. Figure S1 presents a diagram of the experimental setup.

2.1.3. Computational Details. First principles calculations were carried out using density functional theory (DFT), with the Becke's three-parameter hybrid functional using the Lee−Yang−Parr correlation functional (B3LYP) method in combination with different basic sets. The superiority of DFT methods over conventional Hartree−Fock methods for the study of fluoro-carbon-oxygenated compounds had previously been demonstrated, and the determination of geometric parameters for this kind of systems yielded accurate results that were tested against gas electron diffraction experiments.[31−33] Because we are interested in the minima of the potential energy surfaces and DFT methods take into account the electron correlation energy only in part,[34] we believe that the 6-31++G(d,p) and 6-311++G(3d,2p) basic sets should be adequate to describe the relative energies for the isomers. Additionally, harmonic vibrational frequencies and zero-point energies (ZPEs) were calculated at the same level of theory to check whether the stationary points obtained were either isomers or first-order transition states. All calculated conformers had only real frequencies. The determination of the Hessian matrix also enabled calculation of the thermochemical quantities for the conformers that were explicitly set at 543 K in the input file of the Gaussian program. The Møller−Plesset expansion truncated at second order (MP2) and the high accuracy energy method Gaussian-4 (G4) were also used for the calculation of the activation energies to achieve a more complete comparison. All symmetry restrictions were turned off in the calculations. Intrinsic reaction coordinate (IRC) calculations were carried out for all the transition states in order to guarantee their connection with the minima in the potential energy surface (PES). All calculations were run with the Gaussian 09 program package.[35]

2.2. General Procedures. Volatile materials were manipulated in a glass vacuum line equipped with two capacitance pressure gauges (0−760 Torr, MKS Baratron; 0−70 mbar, Bell and Howell), three U traps, and valves with poly(tetrafluoroethylene) stems (Young, London). The vacuum line was connected directly to the stainless steel IR gas cell (total volume equal to 148 mL), placed in the sample compartment of the FTIR instrument (Figure S1). After passivating all the surfaces of the cell with CF_2O at 600 K for 30 min, different pressures of the reactants were loaded in the reaction cell in order to generate the pseudo-first-order plots. The experiment was repeated at different temperatures in the range 513−573 K. The products obtained were identified and quantified from the reference spectra of pure samples.

2.3. Chemicals. The synthesis of CF_2O was carried out by the photolysis of $(CF_3C(O))_2O$ (~50 mbar) in 500 mbar of O_2 (>99.9%, Air Liquide). The photoreactor consisted of a one-neck 12 L glass round-bottom flask with a 30 cm long double-walled water-jacketed quartz tube inside, in which a 40 W low-pressure mercury lamp (Heraeus, Hanau) was placed. CF_2O was purified by vacuum distillation.[29] The compound $CF_3C(O)OH$ was obtained from commercial sources (99%, anhydrous) and used without further purification.

3. RESULTS AND DISCUSSION

Prior to the start of our mechanistic analysis, it is necessary to discard the possible reactions of the reagents themselves. The measured activation energy for the concerted unimolecular thermal decomposition of $CF_3C(O)OH$ found by Ashworth and Harrison was 114 ± 7 kJ mol^{-1}, and the products were CF_3H and CO_2.[20] Because this is an unexpectedly low activation energy and CO_2 production occurred in an irregular manner, they proposed a mechanism involving the formation and subsequent decomposition of adsorbed species on the internal walls of the infrared cell rather than a homogeneous gas-phase reaction. They found an appreciable velocity of decomposition above 575 K. In the present case, the reactions were studied at lower temperatures, and we checked the unimolecular decomposition of the acid by the amount of CF_3H formed in several mixtures of CF_2O and $CF_3C(O)OH$. We found indeed very low amounts of CF_3H that steadily decreased when the partial pressure of CF_2O increased, eventually reaching the point where no CF_3H was observed at all by FTIR. This condition was achieved for concentration ratios $[CF_2O]_0/[CF_3C(O)OH]_0 > 1.5$. Thus, the unimolecular decomposition of the acid under our experimental conditions is discarded. Considering the expression for the rate constant found by Gangloff et al. for the thermal decomposition of CF_2O,[18] $k_{(CF_2O)} = 2.96 \times 10^{-10}\ e^{-38850.1/T}$ [s^{-1}], the half-life of CF_2O in our system is approximately 1043 s, so it can be concluded that almost no CF_2O should decompose by a unimolecular channel in our experiments.

In addition, Table 1 presents the bond dissociation energies for TFA and CF_2O molecules calculated directly using the G4 method. For example, eq 1 was used to calculate the (O−H) dissociation energy:

Table 1. Dissociation Energies for the Unimolecular Rupture of $CF_3C(O)OH$ and CF_2O Calculated at the G4 Level of Theory

dissociation reaction	enthalpy (kJ/mol)
$CF_3C(O)OH \rightarrow CF_3C(O)O + H$	ΔH = +488.0
$CF_3C(O)OH \rightarrow CF_3 + C(O)OH$	ΔH = +359.3
$CF_3C(O)OH \rightarrow CF_3 + CO_2 + H$	ΔH = +376.8
$C(O)F_2 \rightarrow C(O)F + F$	ΔH = +526.1

$$D°[CF_3C(O)O{-}H] = H°[CF_3C(O)O] + H°[H] - H°[CF_3C(O)OH] \quad (1)$$

All single bond scission reactions for $CF_3C(O)OH$ and CF_2O have substantially higher barriers, >200 kJ mol^{-1}, than the molecular processes described later in this work; therefore, no competitive channels are expected for the bimolecular thermal reaction between $CF_3C(O)OH$ and CF_2O.

DOI: 10.1021/acs.jpca.9b00899
J. Phys. Chem. A XXXX, XXX, XXX−XXX

3.1. Reaction Mechanism. In order to determine the products of the reaction, a mixture of (14.5 ± 0.1) mbar of CF_2O and (10.1 ± 0.1) mbar of $CF_3C(O)OH$ was loaded into the stainless steel IR gas cell at 543 K. The sample was interrogated with IR spectra every 40 s intervals. Figure 1

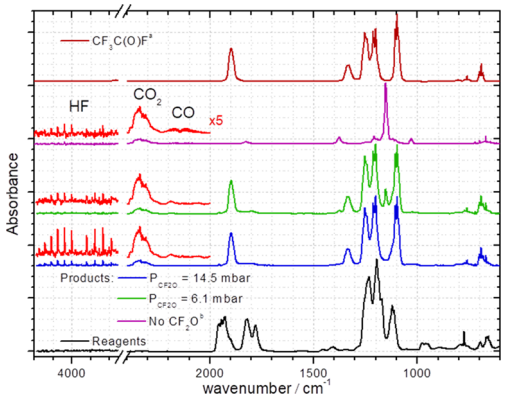

Figure 1. Spectra of the reagents, ($CF_3C(O)OH$ + CF_2O), and products after 3600 s at 543 K (blue spectra correspond to $[CF_2O]/[CF_3C(O)OH]$ = 1.44 and the green spectra to $[CF_2O]/[CF_3C(O)OH]$ = 0.60. [a]$CF_3C(O)F$ spectra were obtained from our own database. [b]The products of the thermal decomposition of $CF_3C(O)OH$ were obtained after 6000 s at 543 K.

shows the spectra of this mixture at zero time (reagents in black line) and at a time sufficiently long so as to consider these to be the final products of the thermal reaction. From the comparison of the products trace with reference spectra from our own inventory, we can conclude that the main products found were HF, CO_2, and $CF_3C(O)F$. When a mixture of (6.1 ± 0.1) mbar of CF_2O and (10.2 ± 0.1) mbar of $CF_3C(O)OH$ was loaded, the products found were mainly the same (HF, CO_2, and $CF_3C(O)F$) with additional small amounts of CO and CF_3H.

Figure 1 also presents the products of the thermal decomposition of $CF_3C(O)OH$ alone measured at the exact same conditions (green line). In this case, the products found were mainly CO_2 and CF_3H (in agreement with Ashworth's proposed mechanism) and very small amounts of CO and HF.[20] Because the products of this reaction are completely different from the ones found in the presence of CF_2O, the thermal title reaction must undergo through a very different mechanism. Numerous series of measurements were made at various constant temperatures including 513, 533, 553, and 573 K. The lowest temperature was set considering kinetic factors because the reaction takes a long time to occur, whereas the highest temperature was chosen on experimental ones because the reaction occurs faster than the time resolution of our FTIR spectrometer. Besides, it should be kept in mind that the thermal decomposition of TFA occurs at an appreciable rate at temperatures higher than 573 K.[20]

The reaction order for CF_2O could be approached upon assumption of first-order behavior from our pseudo-first-order data by plotting the logarithm of the relative concentration of CF_2O (integration of the band 1980−1870 cm^{-1}) as a function of the initial concentration of $CF_3C(O)OH$, evaluated at a fixed reaction time of 1080 s according to eq 2. This procedure was repeated for the four temperatures. All the data are shown in Figure S2.

$$\ln([CF_2O]) = -k\cdot[CF_3C(O)OH]_0\cdot 1080\ \text{s} + \ln([CF_2O]_0) \quad (2)$$

This presentation, plus the fact that the temperature-dependent Arrhenius plots (which are integrated from a first-order dependence on CF_2O and on $CF_3C(O)OH$) also show excellent consistency (Figures 2−4), all points to the total second-order gas-phase reaction.

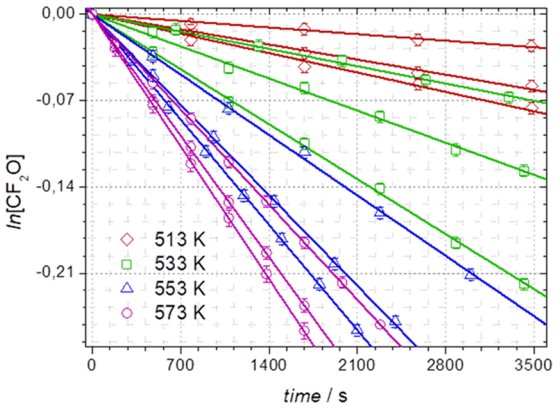

Figure 2. Plot of the time dependence of the CF_2O concentration with different pressures of $CF_3C(O)OH$ in the temperature range 513−573 K (brown ♦ 513 K, green ■ 533 K, blue ▲ 553 K, violet ● 573 K). The $CF_3C(O)OH$ concentrations are indicated in Table 2 with an asterisk. The straight lines are least-squares fits; correlation coefficients are ≥0.996.

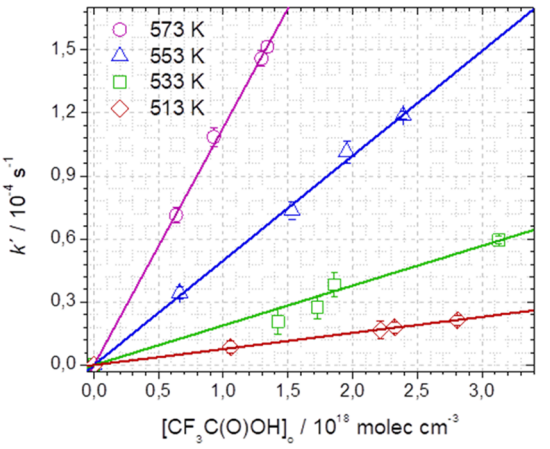

Figure 3. Pseudo-first-order rate constants vs the initial concentration of $CF_3C(O)OH$ at the different temperatures.

3.2. Rate Data at Different Temperatures. In order to determine the behavior of the reaction rate constant as a function of temperature, pseudo-first-order rate constants were obtained from the time evolution of the CF_2O concentration, as shown in Figure 2, for the different temperatures 513, 533, 553, and 573 K. Four experiments were performed by varying the initial concentration of $CF_3C(O)OH$ at each temperature. A good linear fit was obtained in all cases with correlation coefficients greater than 0.996. The results are summarized in Table 2 for the different experimental conditions. As can be noticed, an increase in the pseudo-first-order rate constant is observed when the initial $CF_3C(O)OH$ concentration rises at all temperatures.

Figure 3 presents the dependence of the pseudo-first-order rate constant with the initial concentration of $[CF_3C(O)OH]_0$.

DOI: 10.1021/acs.jpca.9b00899
J. Phys. Chem. A XXXX, XXX, XXX−XXX

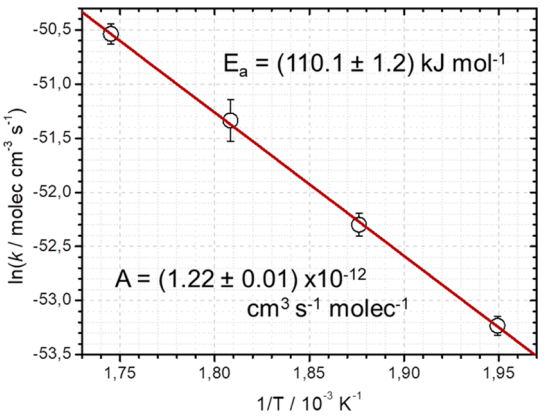

Figure 4. Dependence of the second-order rate constant k upon temperature. Activation energy and pre-exponential factor are derived from the slope and intercept, respectively. The specific reaction rate constant for the process is $k = 1.22 \times 10^{-15} \exp(-13\,250\ [\text{kJ K}]/T)$ [dm^3 molec^{-1} s^{-1}].

Again, good linear regressions were obtained for the different temperatures. This is an indication that the reaction is first-order for $CF_3C(O)OH$ as well, and from the slope, we can obtain the absolute second-order rate constants for the whole process, which are presented in Table 2. The uncertainties were taken considering the standard deviation of the linear regression in Figure 3, the deviation of the pseudo-first-order rate constants, and the initial concentrations of $CF_3C(O)OH$. The rate equation for this reaction is

$$\text{d}[CF_2O]/\text{d}t = k\cdot[CF_2O]\cdot[CF_3C(O)OH] \quad (3)$$

On the basis of the criteria described, Figure 4 shows the Arrhenius plot constructed from the values listed in Table 2. The line in the figure is a least-squares fit to the experimental data. It is seen that the deviation from a straight line is small. From the slope and intercept of the line, a value for the activation energy of $E_a = (110.1 \pm 1.2)$ kJ mol^{-1} and a pre-exponential factor of $A = (1.22 \pm 0.07) \times 10^{-12}$ cm^3 s^{-1} molec^{-1} were obtained, where the uncertainties are the standard errors of the fit. Our recommended expression is $k(T) = (1.2 \pm 0.2) \times 10^{-12} \exp[(110 \pm 6)\ \text{kJ mol}^{-1}/RT]$ cm^3 molec^{-1} s^{-1}, which incorporates our estimated accuracy over the temperature range of the measurements and the uncertainty in the rate constants.

This E_a is slightly lower than the E_a for the heterogeneous thermal decomposition of $CF_3C(O)OH$,[20] and the value of the pre-exponential factor is consistent with a bimolecular homogeneous gas-phase reaction.[36−38] We can think the mechanism as a stepwise two-reaction mechanism from these reagents to produce $CF_3C(O)F$, HF, and CO_2

$$CF_2O + CF_3C(O)OH \rightarrow CF_3C(O)OC(O)F + HF \quad (4)$$

$$CF_3C(O)OC(O)F \rightarrow CF_3C(O)F + CO_2 \quad (5)$$

The formation of the intermediate, $CF_3C(O)OC(O)F$, must be considered to explain the production of $CF_3C(O)F$. To the best of our knowledge, this molecule is unknown. Once the intermediate is formed, the mechanism proceeds through its thermal decomposition. Considering the above mechanism and assuming the steady-state approximation for the intermediate, the velocity of the reaction is given by the equation $v = k_1k_2[CF_2O][CF_3C(O)OH]/k_{-1}[HF] + k_2$. As the kinetic parameters were obtained at the first stages of reaction where the HF concentration is low, we can approximate $k_{-1}[HF] < k_2$ and the rate law is given by eq 3 with $k = k_1$.

3.3. First Principles Calculations. Perfluorinated acids are known to form dimers because of the two hydrogen bonds that could be formed from the acid group. Hess et al. studied the thermodynamics of the dissociation for the $CF_3C(O)OH$ dimer, in which the enthalpy $H_{diss} = 59.7 \pm 0.7$ kJ mol^{-1} and the entropy $S_{diss} = 155 \pm 2$ J mol^{-1} K^{-1}.[39] To explore the possibility of hydrogen-bond formation in our system between the pairs $CF_3C(O)OH\cdots OCOHCF_3$ and $CF_3C(O)OH\cdots FFC(O)$, a relaxed PES scan of the X···H bond distance from 1.4 to 6.1 Å using the UB3LYP method was run with tight convergence optimizations (the calculations converged normally for all points). Figure S3 presents the energy as a function of X−H distance (where X = O or F). A calculation of

Table 2. Pseudo-First-Order Rate Constants and Derived Rate Constants for the Thermal Reaction between $CF_3C(O)OH$ and CF_2O

	initial concentrations[a] (molec cm^{-3})			
temperature (K)	$CF_3C(O)OH$	CF_2O	pseudo-first-order rate constants (s^{-1})	rate constant (cm^3 molec^{-1} s^{-1})
573	6.36×10^{17}	1.39×10^{17}	$(7.14 \pm 0.12) \times 10^{-5}$	$(1.13 \pm 0.15) \times 10^{-22}$ (for 4 exp)
	[b]9.27×10^{17}	1.46×10^{17}	$(1.09 \pm 0.15) \times 10^{-4}$	
	[b]1.30×10^{18}	1.40×10^{17}	$(1.46 \pm 0.12) \times 10^{-4}$	
	[b]1.34×10^{18}	1.53×10^{17}	$(1.52 \pm 0.10) \times 10^{-4}$	
553	6.63×10^{17}	1.39×10^{17}	$(3.45 \pm 0.09) \times 10^{-5}$	$(5.07 \pm 0.38) \times 10^{-23}$ (for 4 exp)
	[b]1.53×10^{18}	1.56×10^{17}	$(7.35 \pm 0.15) \times 10^{-5}$	
	[b]1.95×10^{18}	1.44×10^{17}	$(1.01 \pm 0.18) \times 10^{-4}$	
	[b]2.39×10^{18}	1.53×10^{17}	$(1.19 \pm 0.06) \times 10^{-4}$	
533	[b]1.42×10^{18}	1.33×10^{17}	$(2.06 \pm 0.20) \times 10^{-5}$	$(1.94 \pm 0.22) \times 10^{-23}$ (for 4 exp)
	1.73×10^{18}	1.58×10^{17}	$(2.74 \pm 0.17) \times 10^{-5}$	
	[b]1.86×10^{18}	1.45×10^{17}	$(3.84 \pm 0.19) \times 10^{-5}$	
	[b]3.12×10^{18}	1.37×10^{17}	$(5.97 \pm 0.05) \times 10^{-5}$	
513	[b]1.06×10^{18}	1.49×10^{17}	$(8.49 \pm 0.10) \times 10^{-6}$	$(7.62 \pm 0.13) \times 10^{-24}$ (for 4 exp)
	2.21×10^{18}	1.65×10^{17}	$(1.66 \pm 0.14) \times 10^{-5}$	
	[b]2.33×10^{18}	1.59×10^{17}	$(1.73 \pm 0.08) \times 10^{-5}$	
	[b]2.81×10^{18}	1.47×10^{17}	$(2.15 \pm 0.08) \times 10^{-5}$	

[a]Concentrations were derived from the pressures measured at room temperature. [b]Concentrations used in Figure 2.

DOI: 10.1021/acs.jpca.9b00899
J. Phys. Chem. A XXXX, XXX, XXX−XXX

the thermodynamics of this dissociation for two $CF_3C(O)OH$ molecules at the G4MP2 level of theory resulted in values similar to those found experimentally by Hess (H_{diss} = 57.5 kJ mol^{-1} and S_{diss} = 154 J mol^{-1} K^{-1}), and considering the formation of hydrogen-bond interaction between the molecules of $CF_3C(O)OH$ and CF_2O, the equivalent ones obtained at the same level of theory were H_{diss} = 9.9 kJ mol^{-1} and S_{diss} = 60 kJ mol^{-1} for the F···H interaction. Under the experimental temperatures, the thermal energy is high enough to overcome the formation of the dimer in the gas phase.

The results of the minima and transition states in the PES for the thermal reaction $CF_3C(O)OH + CF_2O$ were calculated at different levels of theory (UB3LYP, MP2, and G4MP2) and are presented in Table 3. An inspection of the values shows

Table 3. Energies of Minima and Transition States of the Energy Reaction Surface for the Reaction between $CF_3C(O)OH$ and CF_2O Calculated at Different Levels of Theory

	B3LYP		MP2	
	6-31++G(d,p)	6-311++G(3df,2pd)	6-31++G(d,p)	G4MP2
TS1−6	107	112	122	114
TS1−4	209	213	214	215
Prod1	34	35	32	18
TS2	131	129	152	130
Prod2	−72	−86	−55	−64

that the energy of TS2 calculated with the MP2 method is very different from the values for G4MP2 and B3LYP, indicating that the electron correlation is important for this TS. However, the energy values found for the other species are similar regardless of the method used. We consider G4MP2 energies to be the most appropriate method for our analysis. The energies at G4MP2 are shown in Scheme 1. As the CF_2O

Scheme 1. Theoretical Calculation of the Most Probable Path for the $CF_3C(O)OH + CF_2O$ Thermal Reaction at the G4MP2 Level of Theory[a]

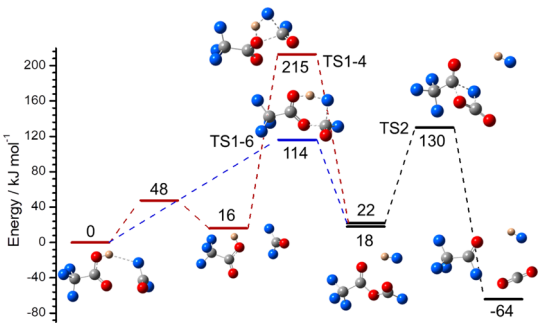

[a]The connection between minimum and TS was corroborated by IRC calculations at B3LYP/6-31++G(d,p).

molecule approaches to the −C(O)OH moiety, a minimum is reached (zero energy in the PES, see Figure S3) from which two pathways for eq 6 on the S_0 surface are possible: the formation of a six-center transition state (TS1−6, more stable) and a four-center transition state (TS1−4) from the trans-conformer of TFA. The theoretical energy barrier for TS1−6 is (114 ± 5) kJ mol^{-1}, where we considered the hydrogen-bond interaction between the two reagents (Figure S3) as the error in the definition of the ZPE. The stability of six-center structures over the four-center ones is well-known for this kind of processes,[6,40] and in our case, the stability is ≈100 kJ mol^{-1} (depending on the method used). The energies along the IRC for the two pathways calculated at the B3LYP level of theory are plotted in Figure 5. In the figure, filled blue circles

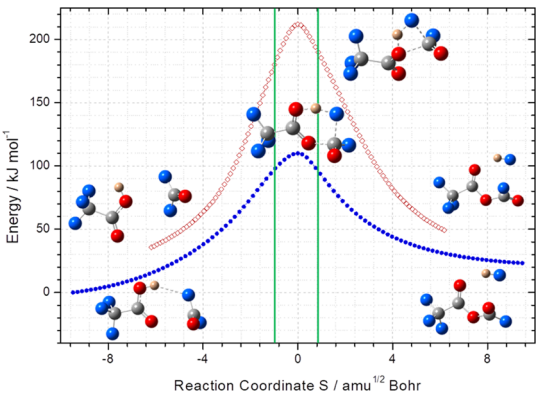

Figure 5. IRC calculation for the six-center (filled blue circles) and four-center transition state (empty red diamonds). The minimum potential energy of $CF_3C(O)OH + CF_2O$ without zero-point correction is chosen as zero. As IRC points were calculated at the B3LYP/6-31++G(d,p) level, the barrier heights are not identical to the G4 results in Scheme 1, even after zero-point correction.

represent the path from the *cis*-TFA conformer through TS1−6, and open red diamonds represent the reaction from the *trans*-TFA conformer through TS1−4, where the energies are given relative to the B3LYP *cis*-TFA conformer + CF_2O. The energy along the reaction coordinate that leads to TS1−6 has a relatively flat plateau in the vicinity of the TS (with $\Delta E \approx 8$ kJ mol^{-1} from $S \approx -1.0$ to $S \approx 0.8$—where S is the internal reaction coordinate defined by G09-), after which the F atom approaches the H atom to eliminate HF. However, for TS1−4, the energy profile seems to be sharper in the vicinity of the TS (with $\Delta E \approx 28$ kJ mol^{-1} from $S \approx -1.0$ to $S \approx 0.8$). This difference between both paths is due in part to the stabilization of the transition state because of the interaction between the carbon atom on CF_2O and the carbonyl oxygen of TFA to form a six-center transition state.

Our calculations predict that the reaction proceeds through the elimination of HF and the formation of the intermediate perfluoroacetic fluoroformic anhydride, $CF_3C(O)OC(O)F$. Because no information about this species was found in bibliography, we performed the characterization of the conformers and their vibrational modes.

A priori the PES of $CF_3C(O)OC(O)F$ can be thought of as having two minima according to the syn/anti positions of the $C_2-O_2-C_3-F_4$ dihedral. These structures are presented in Figure S4, where the conformer syn is 3.81 kJ mol^{-1} more stable than the anti. By considering this difference in the relative energies, under the experimental conditions (543 K), the populations calculated for a typical Boltzmann distribution are 56.3% syn and 43.7% anti. The vibrational frequencies for both conformers obtained at the DFT-B3LYP/6-311++G-(3df,2pd) level of theory are presented in Table S2. All 24 fundamental modes should be both IR- and Raman-active, and all the vibrational frequencies are real and positive. The frequencies and intensities (relative IR band intensities in parentheses) obtained for both conformers present differences in the F−C═O stretching bands, but the other bands coincide

DOI: 10.1021/acs.jpca.9b00899
J. Phys. Chem. A XXXX, XXX, XXX−XXX

quite well. The assignments shown in the last column of the table were done from the evaluation of the normal mode displacement vectors; as many of the modes are strongly coupled, this information is rather subjective.

Figure 6a presents the calculated IR spectra of the traces because of the syn (blue line) and anti (green line)

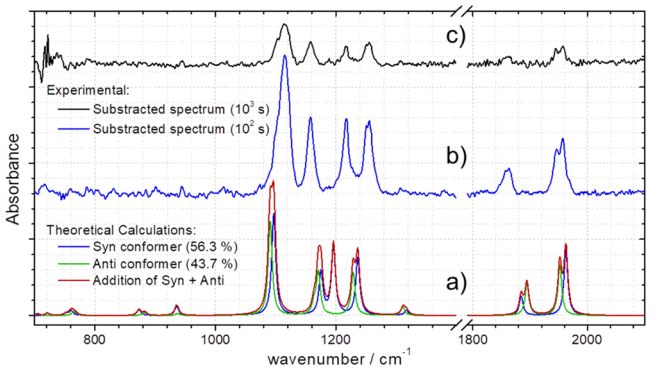

Figure 6. (a) Calculated spectra of the two more stable conformers of $CF_3C(O)OC(O)F$ (B3LYP/6-311++G(3df,2pd)); (b,c) experimental spectra (100 and 1000 s, respectively, at 543 K) after the subtraction of all the reagents and products (CF_2O, $CF_3C(O)OH$, $CF_3C(O)F$, CO_2, HF, and CO).

conformers, which in turn conform the simulated spectrum (red line) weighted for their contributions of 56.3 and 43.7%, respectively. Our kinetic simulations (that will be discussed later) predict that this intermediate reaches the maximum concentration around 100 s after the start of the thermal reaction at 543 K. Therefore, the analysis of the experimental spectrum after 100 s should show some characteristic bands of this intermediate. Furthermore, the subtraction of the spectra of reagents and products leads to the spectrum of Figure 6b, which shows characteristic bands corresponding to the C═O symmetric stretching vibrations between 1940 and 1964 cm^{-1} and asymmetric stretching between 1873 and 1892 cm^{-1}; the CF_3 asymmetric bending at ≈1229 and 1171 cm^{-1}; the F−C−O asymmetric stretching band at ≈1199 cm^{-1}; and the C−O−C asymmetric stretching vibration between 1073 and 1108 cm^{-1}. The similarities between the simulated theoretical spectrum and the experimental one are clear. The position and intensity of the bands are also compared in Table S1. These bands are also observed weakly in the spectrum of Figure 6c, which would correspond to the intermediate after 1000 s of reaction.

After elimination of HF, the intermediate $CF_3C(O)OC(O)F$ can decompose into $CF_3C(O)F$ and CO_2 with a barrier energy of 130 kJ mol^{-1} relative to the reagents, higher than that of TS1−6. The back reaction −1, which presents an energy barrier of 92 kJ mol^{-1}, would be important only when the concentration of $CF_3C(O)OC(O)F$ and HF would be high. However, in our experimental conditions, the amount of these species is believed to be low enough to discard the back reaction. Thus, once the syn/anti intermediate is formed, the unimolecular decomposition would be favored in terms of the velocities. According to the calculations, it proceeds through a concerted step and a four-center TS (TS2, as shown in Scheme 1, and postulated in reaction 5). Thus, the final product would be $CF_3C(O)F$, HF, and CO_2 as it was observed in the spectra of Figure 1.

3.4. Thermochemical Kinetic Parameters.

The activation enthalpy ($\Delta H^{\ddagger}$), entropy ($\Delta S^{\ddagger}$), and Gibbs free energy ($\Delta G^{\ddagger}$) were derived from the experimental Arrhenius parameters at 543 K.

Table 4 summarizes these experimental values, and the equivalent values obtained by ab initio calculations at the

Table 4. Arrhenius Parameters and the Derived Thermodynamics Values from the Activation Energy of the Thermal Reaction between $CF_3C(O)OH$ and CF_2O at 543 K

	experimental	calculated[a]
A (cm^3 $molec^{-1}$)	$(1.2 \pm 0.2) \times 10^{-12}$	$(1.9 \pm 0.8) \times 10^{-12}$
E_a (kJ mol^{-1})	110.1 ± 6.1	114 ± 5
$\Delta H^{\ddagger}$ (kJ mol^{-1})	105.6 ± 6.4	110 ± 5
$\Delta S^{\ddagger}$ (J mol^{-1})	−88.6 ± 9.7	−81 ± 4
$\Delta G^{\ddagger}$ (kJ mol^{-1})	153.7 ± 13.5	155 ± 7

[a]Calculations at the G4MP2 level of theory for TS1−6.

G4MP2 level of theory for the TS1−6 transition state. Considering the errors, the values are in very good agreement. The rate constant at this temperature was derived from the $\Delta G^{\ddagger}$ value, according to eq 6, to be $k_1(543\ K) = (2.9 \pm 2.3) \times 10^{-23}$ cm^3 $molec^{-1}$ s^{-1}.

$$k(T) = \frac{k_b T}{hc^0} e^{-\Delta^{\ddagger} G^0/RT} \quad (6)$$

From this rate constant, we were able to calculate the pre-exponential factor $A = (1.9 \pm 0.8) \times 10^{-12}$ cm^3 $molec^{-1}$, which agrees with the experimental one (Table 4). The similarity between the experimental and calculated entropies confirms the formation of an ordered transition state for reaction 4, and the calculated A value confirms that the homogenous reaction takes place in the gas phase.

The calculation of the rate constants for reactions −1 and 5 was also carried out on a similar basis, being $k_{-1}(543\ K) = 2.6 \times 10^{-22}$ cm^3 $molec^{-1}$ s^{-1} and $k_2(543\ K) = 0.034$ s^{-1}, which confirms that k_1 is the rate-determining step under our experimental conditions. A kinetic simulation was carried out taking into account only these reactions. The results are presented in Figure 7 as the relative concentration (continuous lines) as a function of time. The figure also presents the normalized experimental concentrations for $CF_3C(O)F$ (1819 cm^{-1} band), CF_2O (1942 cm^{-1} band), CO_2 (integrated band between 2375 and 2281 cm^{-1}), and $CF_3C(O)F$ (integrated between 1355 and 1312 cm^{-1}), comparing all of them with calibrations of our repository. Quantitative analysis for the production of HF was not possible because the vibro-rotational bands are very sharp, and the integration resulted in unreliable values. In the same way, it was impossible to record the presence of the intermediate over time because the stronger bands of this compound overlap with those of CF_2O, $CF_3C(O)OH$, and $CF_3C(O)F$. However, we were able to estimate its relative concentration for t = 100, 1000 s after assuming a cross section similar to that of $CF_3C(O)F$ though we know this estimation will have a 50% error associated. As mentioned previously, the maximum concentration of this intermediate is reached about 100 s from the beginning of reaction (Figure 7). In order to corroborate the hypothesis that reaction −1 is negligible in our experimental conditions, the simulation was run with different amounts of HF added. Figure S5 shows the disappearance of CF_2O for two initial

DOI: 10.1021/acs.jpca.9b00899
J. Phys. Chem. A XXXX, XXX, XXX−XXX

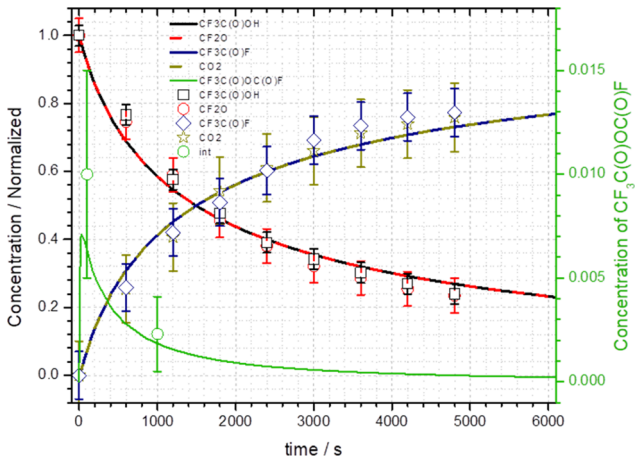

Figure 7. Reaction progression at 543 K: lines correspond to the simulated concentration over time (calculated rated constants were used). Dots correspond to the measured relative concentrations of each species over time.

concentrations of the reagents. In panel a, $[CF_2O]_i \approx 1.5 \times 10^{17}$ and $[CF_3C(O)OH]_i \approx 1.5 \times 10^{18}$ molec cm^{-3}, and in panel b, $[CF_2O]_i \approx 2.0 \times 10^{19}$ and $[CF_3C(O)OH]_i \approx 2.0 \times 10^{18}$ molec cm^{-3}. For both conditions, the initial HF concentration varied from 0.5 to 100 times the CF_2O. It is clearly seen that the disappearance of CF_2O is only affected when the amount of HF exceeds the initial concentration of CF_2O. This indicates that although the activation energy for reaction 5 is slightly higher than for 4 as indicated in Scheme 1, at the present conditions the overall reaction is dominated by the velocity of reaction 4.

Even though it is difficult to isolate the anhydride $CF_3C(O)OC(O)F$, we were able to estimate its half-life at room temperature from the rate constant found at 543 K by G4MP2 calculations ($k_2 = 0.034$ s^{-1}; $t_{1/2} = 20.3$ s), while the value at room temperature is $k_2(298\ K) = 2.3 \times 10^{-12}$ s^{-1}.

4. CONCLUSIONS

The two compounds involved in this reaction have very long stratospheric half-lives. In fact, CF_2O is such a stable molecule that its concentration is growing steadily especially at high altitudes.[41] Similar conclusions could be thought for $CF_3C(O)OH$ that escapes the wet deposition of the troposphere. Even so, its mutual reaction is too slow at tropospheric conditions and could become considerable only with growing concentrations and altitudes. In the temperature range 513−573 K, it proceeds homogeneously in the gas phase through the formation of a reaction intermediate, here characterized as $CF_3C(O)OC(O)F$, the final products being $CF_3C(O)F$, HF, and CO_2. The reaction is first-order respect to each reagent, and second order global and proceeds via a concerted step through a six-center transition state with experimental $E_a = 110.1 \pm 6.1$ kJ mol^{-1} and $A = (1.2 \pm 0.2) \times 10^{-12}$ cm^3 $molec^{-1}$ s^{-1}. This TS is facilitated by the hydrogen-bond interactions between the −OH group of the acid and the F atom of the CF_2O. Some thermodynamic activation values were also found for this reaction: $\Delta H^{\ddagger} = 105.6 \pm 6.4$ kJ mol^{-1}, $\Delta S^{\ddagger} = -88.6 \pm 9.7$ J mol^{-1} K^{-1}, and $\Delta G^{\ddagger} = 153.7 \pm 13.5$ kJ mol^{-1}. The comparison with ab initio calculations at the G4MP2 level of theory showed excellent similarities, thus proving the proposed mechanism.

■ ASSOCIATED CONTENT

Supporting Information

The Supporting Information is available free of charge on the ACS Publications website at DOI: 10.1021/acs.jpca.9b00899.

Materials concerning the experimental setup, test for reaction order, energy of the hydrogen bond, syn and anti conformers of the intermediate $CF_3C(O)OC(O)F$, kinetic simulation of the reaction under different $[HF]_i$, and experimental and calculated vibrational modes for the two more stable conformers of $CF_3C(O)OC(O)F$ (PDF)

■ AUTHOR INFORMATION

Corresponding Author

*E-mail: mburgos@fcq.unc.edu.ar.

ORCID

Maxi A. Burgos Paci: 0000-0003-2002-7481

Author Contributions

The manuscript was written through contributions of all authors. All authors have given approval to the final version of the manuscript.

Notes

The authors declare no competing financial interest.

■ ACKNOWLEDGMENTS

Financial support from Consejo Nacional de Investigaciones Científicas y Técnicas (CONICET), FONCyT, and SECyT-UNC is gratefully acknowledged.

■ REFERENCES

(1) Raper, O. F.; Farmer, C. B.; Zander, R.; Park, J. H. Infrared spectroscopic measurements of halogenated sink and reservoir gases in the stratosphere with the ATMOS instrument. *J. Geophys. Res.* **1987**, *92*, 9851−9856.

(2) World Meteorological Organisation. *Global Ozone Research and Monitoring Project - Report No. 20, Scientific Assessment of Stratospheric Ozone*, 1989; Vol. *II*, Appendix: AFEAS Report, pp 161−266.

(3) Modiano, S. H.; McNesby, K. L.; Marsh, P. E.; Bolt, W.; Herud, C. Quantitative Measurements by Fourier Transform Infrared Spectroscopy of Toxic Gas Production During Inhibition of JP-8 Fires by CF_3Br and $C_3F_7H_1$. *Appl. Opt.* **1996**, *35*, 4004−4008.

(4) *The Merck Index*, 13th ed; O'Neil, M. J., Ed.; Whitehouse Station, NJ: Merck & Co., 2001; p 1725.

(5) Kotamarthi, V. R.; Rodriguez, J. M.; Ko, M. K. W.; Tromp, T. K.; Sze, N. D.; Prather, M. J. Trifluoroacetic acid from degradation of HCFCs and HFCs: A three-dimensional modeling study. *J. Geophys. Res.* **1998**, *103*, 5747−5758.

(6) Berasategui, M.; Argüello, G. A.; Burgos Paci, M. A. Thermal Decomposition of $FC(O)OCH_3$ and $FC(O)OCH_2CH_3$. *Phys. Chem. Chem. Phys.* **2018**, *20*, 12817−12826.

(7) Kaye, J. A.; Douglass, A. R.; Jackman, C. H.; Stolarski, R. S.; Zander, R.; Roland, G. Two-dimensional model calculation of fluorine-containing reservoir species in the stratosphere. *J. Geophys. Res.* **1991**, *96*, 12865−12881.

(8) Francisco, J. S.; Maricq, M. M. Atmospheric Photochemistry of Alternative Halocarbons. *Advances in Photochemistry*, 1995; Vol. *20*, pp 79−163.

(9) Christensen, L. K.; Wallington, T. J.; Guschin, A.; Hurley, M. D. Atmospheric Degradation Mechanism of CF_3OCH_3. *J. Phys. Chem. A* **1999**, *103*, 4202−4208.

(10) Goto, M.; Kawasaki, M.; Wallington, T. J.; Hurley, M. D.; Sharratt, A. P. Atmospheric Chemistry of CH_2FOCH_2F: Reaction with Cl Atoms and Atmospheric Fate of $CH_2FOCHFO\cdot$ radicals. *Int. J. Chem. Kinet.* **2002**, *34*, 139−147.

DOI: 10.1021/acs.jpca.9b00899
J. Phys. Chem. A XXXX, XXX, XXX−XXX

(11) Wallington, T. J.; Ellermann, T.; Nielsen, O. J.; Sehested, J. Atmospheric Chemistry of FCO_x Radicals: UV Spectra and Self-Reaction Kinetics of FCO and $FC(O)O_2$ and Kinetics of Some Reactions of FCO_x with O_2, O_3, and NO at 296 K. *J. Phys. Chem.* **1994**, *98*, 2346−2356.
(12) Fockenberg, Ch.; Saathoff, H.; Zellner, R. A Laser Photolysis/LIF Study of the Rate Constant for the Reaction $CF_3O + O_3 \rightarrow$ Products. *Chem. Phys. Lett.* **1994**, *218*, 21−28.
(13) Wallington, T. J.; Ball, J. C. Atmospheric Chemistry of CF_3O Radicals: Reaction with O_3. *Chem. Phys. Lett.* **1995**, *234*, 187−194.
(14) Arvía, A. J.; Aymonino, P. J.; Schumacher, H. J. Preparation and Properties of Bis-(Monofluorocarbonyl) Peroxide. *An. Asoc. Quim. Argent.* **1962**, *50*, 135−143.
(15) Berasategui, M.; Argüello, G. A.; Burgos Paci, M. A. Reaction of Methyl Fluoroformyl Peroxycarbonate ($FC(O)OOC(O)OCH_3$) with Cl Atoms: Formation of Hydro-ChloroFluoro-Peroxides. *J. Phys. Chem. A* **2017**, *121*, 7469−7476.
(16) Argüello, G. A.; Willner, H.; Malanca, F. E. Reaction of CF_3 Radicals with CO and O_2. Isolation of Bis(trifluoromethyl)-peroxydicarbonate, $CF_3OC(O)OOC(O)OCF_3$, and Identification of Bis(trifluoromethyl)trioxydicarbonate, $CF_3OC(O)OOOC(O)OCF_3$. *Inorg. Chem.* **2000**, *39*, 1195−1199.
(17) Argüello, G. A.; Willner, H. IR and UV Absorption Spectrum of the Trifluoromethoxy Radical, $CF_3O\cdot$, Isolated in Rare Gas Matrices. *J. Phys. Chem. A* **2001**, *105*, 3466−3470.
(18) Gangloff, H. J.; Milks, D.; Maloney, K. L.; Adams, T. N.; Matula, R. A. An Experimental and Mechanistic Study of the Reactions of COF_2 with H_2 and with CO. *J. Chem. Phys.* **1975**, *63*, 4915−4926.
(19) Modica, A. P. Chemical Kinetics of Carbonyl Fluoride Decomposition in Shock Waves. *J. Phys. Chem.* **1970**, *74*, 1194−1204.
(20) Ashworth, A.; Harrison, P. G. Fourier-Transform Infrared Study of the Gas-Phase Thermolysis of Trifluoroacetic Acid. *J. Chem. Soc. Faraday Trans.* **1993**, *89*, 2409−2412.
(21) Wallington, T. J.; Hurley, M. D. Atmospheric Chemistry of CF_3COOH: Kinetics of Fluorine and Chlorine Atom Reaction at 295 ± 2 K. *Int. J. Chem. Kinet.* **1995**, *27*, 189−194.
(22) Kazil, J.; McKeen, S.; Kim, S.-W.; Ahmadov, R.; Grell, G. A.; Talukdar, R. K.; Ravishankara, A. R. Deposition and Rainwater Concentrations of Trifluoroacetic Acid in the United States from the Use of HFO-1234yf. *J. Geophys. Res. Atmos.* **2014**, *119*, 14059−14079.
(23) Wang, Z.; Wang, Y.; Li, J.; Henne, S.; Zhang, B.; Hu, J.; Zhang, J. Impacts of the Degradation of 2,3,3,3-Tetrafluoropropene into Trifluoroacetic Acid from Its Application in Automobile Air Conditioners in China, the United States, and Europe. *Environ. Sci. Technol.* **2018**, *52*, 2819−2826.
(24) von Ahsen, S.; Willner, H.; Burgos Paci, M. A.; García, P.; Argüello, G. A. The Open-Chain Trioxide $CF_3OC(O)OOOC(O)OCF_3$. *Chem.—Eur. J.* **2003**, *9*, 5135−5141.
(25) Pernice, H.; Berkei, M.; Henkel, G.; Willner, H.; Argüello, G. A.; McKee, M. L.; Webb, T. R. Bis(fluorformyl)trioxid, FC(O)-OOOC(O)F. *Angew. Chem.* **2004**, *116*, 2903−2906.
(26) Burgos Paci, M. A.; García, P.; Malanca, F. E.; Argüello, G. A.; Willner, H. Synthesis and Characterization of Trifluoromethyl Fluoroformyl Peroxycarbonate, $CF_3OC(O)OOC(O)F$. *Inorg. Chem.* **2003**, *42*, 2131−2135.
(27) Bossolasco, A. G.; Vila, J. A.; Burgos Paci, M. A.; Malanca, F. E.; Argüello, G. A. A new perfluorinated peroxynitrate, $CF_3CF_2CF_2CF_2OONO_2$. Synthesis, Characterization and Atmospheric Implications. *Chem. Phys.* **2014**, *441*, 11−16.
(28) Burgos Paci, M. A.; Argüello, G. A. Kinetics of the Reaction between CF_2O and CH_3OH. *Environmental Simulation Chambers: Application to Atmospheric Chemical Processes*; Springer, 2006; pp 207−212.
(29) Berasategui, M.; Burgos Paci, M. A.; Argüello, G. A. Isolation and Characterization of $CH_3OC(O)OOC(O)F$ from the Reaction CH_3OH + $FC(O)OOC(O)F$. *Z. Anorg. Allg. Chem.* **2012**, *638*, 547−552.
(30) Berasategui, M.; Burgos Paci, M. A.; Argüello, G. A. Properties and Thermal Decomposition of the Hydro-Fluoro-Peroxide CH3OC-(O)OOC(O)F. *J. Phys. Chem. A* **2014**, *118*, 2167−2175.
(31) Mack, H.-G.; Oberhammer, H.; Védova, C. O. D. Bis-(fluorocarbonyl) Peroxide; an Unusual Molecular Structure. *Angew. Chem., Int. Ed. Engl.* **1991**, *30*, 1145−1146.
(32) Kopitzky, R.; Willner, H.; Hermann, A.; Oberhammer, H. Bis(trifluoroacetyl) Peroxide, $CF_3C(O)OOC(O)CF_3$. *Inorg. Chem.* **2001**, *40*, 2693−2698.
(33) Hnyk, D.; Macháček, J.; Argüello, G. A.; Willner, H.; Oberhammer, H. Stucture and Conformational Properties of Bis-(trifluoromethyl) Peroxydicarbonate, $CF_3OC(O)O$-$OC(O)OCF_3$. *J. Phys. Chem. A* **2003**, *107*, 847−851.
(34) Lee, C.; Yang, W.; Parr, R. G. Development of the Colle-Salvetti Correlation-Energy Formula into a Functional of the Electron Density. *Phys. Rev. B: Condens. Matter Mater. Phys.* **1988**, *37*, 785−789.
(35) Frisch, M. J.; Trucks, G. W.; Schlegel, H. B.; Scuseria, G. E.; Robb, M. A.; Cheeseman, J. R.; Scalmani, G.; Barone, V.; Mennucci, B.; Petersson, G. A.; et al. *Gaussian 09*, Revision A.02; Gaussian, Inc.: Wallingford, CT, 2009.
(36) Vetters, B.; Dils, B.; Nguyen, T. L.; Vereecken, L.; Carl, S. A.; Peeters, J. Absolute Rate Coefficients over Extended Temperature Ranges and Mechanisms of the $CF(X^2\Pi)$ Reactions with F_2, Cl_2 and O_2. *Phys. Chem. Chem. Phys.* **2009**, *11*, 4319−4325.
(37) Tajima, S.; Hayashi, T.; Hori, M. Evaluation of the Difference in the Rate Coefficients of $F_2 + NO_x$ (x = 1 or 2) → F + FNO_x by the Stereochemical Arrangement Using the Density Functional Theory. *J. Phys. Chem. A* **2015**, *119*, 1381−1387.
(38) Buendía-Atencio, C.; Pieffet, G. P.; Croce, A. E.; Cobos, C. J. Theoretical Kinetic Study of the Reaction of SF_5 Radical with F_2, Cl_2 and SF_5. *Comp. and Theor. Chem.* **2016**, *1090*, 41−46.
(39) Sauren, H.; Winkler, A.; Hess, P. Kinetics and energetics of hydrogen bond dissociation in isolated acetic acid-d1 and -d4 and trifluoroactic acid dimers. *Chem. Phys. Lett.* **1995**, *239*, 313−319.
(40) Mane, R. B.; Rao, G. S. K. Studies in terpenoids. Part XXIII. An approach to the 1-aryl-1,2,2-trimethylcyclopentane skeleton by intramolecular ketocarbene insertion. Synthesis of β-cuparenone. *J. Chem. Soc., Perkin Trans. 1* **1973**, 1806−1808.
(41) Zander, R.; Rinsland, C. P.; Mahieu, E.; Gunson, M. R.; Farmer, C. B.; Abrams, M. C.; Ko, M. K. W. Increase of Carbonyl Fluoride (COF_2) in the Stratosphere and Its Contribution to the 1992 Budget of Inorganic Fluorine in the Upper Stratosphere. *J. Geophys. Res. Atmos.* **1994**, *99*, 16737−16743.

DOI: 10.1021/acs.jpca.9b00899
J. Phys. Chem. A XXXX, XXX, XXX−XXX